Materials Science-Poland, 40(3), 2022, pp. 64-71
http://www.materialsscience.pwr.wroc.pl/
DOI: 10.2478/msp-2022-0031

Microstructure and mechanical properties of selective laser melted 18Ni300 steel

Yan Liang[1,2], Luo Qing[3,*], He Yu[4], Zhao Huili[5], Wang Yuxin[1,†]

[1]Dept. of Material Science and Engineering, School of Materials Science and Engineering, Jiang Su University of Science and Technology, zhenjiang 212100, China

[2]Dept. of Material Science and Engineering, School of Intelligent Manufacturing and Control Engineering, Shanghai Polytechnic University, Shanghai 201209, China

[3]Dept. of General Dentistry, Shsnghai Xuhui District Dental Center, Shanghai 200031, China

[4]Cancer Center, Xinhua Hospital Affiliated to Shanghai Jiao Tong University School of Medicine, Shanghai 200092, China

[5]Nursing Department, Xinhua Hospital Affiliated to Shanghai Jiao Tong University School of Medicine, Shanghai 200092, China

The energy transfer process of selective laser melting (SLM) is highly complex. In this work, experiments were carried out to study the effects of SLM on the microstructure and mechanical properties of 18Ni300 martensitic steel. With the increase in laser power, the grain size of the cladding layer decreases and the microstructure becomes dense. The side hardness is higher than upper surface hardness, and the tensile strength and elongation both increase first and then decrease. When the laser power is 300 W and the scanning speed is 1,000 mm/s, the comprehensive mechanical properties are the best, as the tensile strength, microhardness, elongation at break, and elongation after fracture are 1,217 MPa, 37.5%, 37.6%, and 8.93%, respectively. EBSD (Electron Backscatter Diffraction) shows that columnar crystals grow along the growth direction (z direction) in XOZ and YOZ planes, and the grains show weak texture. There are many small-angle grain boundaries, and the grain sizes are <10 μm.

Keywords: *selective laser melting, 18Ni300, temperature field, grain size*

1. Introduction

Martensitic steel is outstanding because of high strength, good toughness, excellent high-temperature mechanical properties, small heat treatment deformation, easy processing, and no decarburization [1, 2]. Thus, it is widely used in aerospace, petrochemical, machinery, and mold industries.

With the development of 3D printing technology, selective laser melting (SLM) has advanced the traditional manufacturing technology. It has no limit on the complex structure of formed parts and can be produced in small batches, saving both production time and cost [3]. When the additive manufacturing technology is used to manufacture engineering parts, the current mainstream technology focuses on steel (low carbon [4], stainless steel [5], dual-phase steel [6], and TC [2]), nickel-based superalloy [7–9], and titanium-based alloy [10–12]. The relevant research on martensitic steel formed by SLM is relatively well-established, focusing on the optimization of the SLM formation process and the microstructure and mechanical properties of the formed parts [13]. Bai et al. [14] used different process parameters to form 18Ni300 martensitic steel by SLM. With the increase in laser energy density, the melting amount of metal powder increased and the spatter of molten liquids was intensified, leading to the formation of pores in the formed parts [15]. Riccardo Casati et al. prepared 18Ni300 maraging steel by SLM and aged the formed parts. The amount of residual austenite after aging treatment changed with aging temperature and aging time [16]. Yang, K. et al. prepared 18Ni300 maraging steel by SLM and aged the formed parts [17]. The microstructure was coarse martensite and was

* E-mail: drlq@163.com
† E-mail: ywan943@163.com

© Liang et al. 2022. This is an open access article distributed under the Creative Commons Attribution-NonCommercial-NoDerivatives 4.0 License. (http://creativecommons.org/licenses/by-nc-nd/4.0/)

Table 1. Comparison of the chemical composition of declared, powder, and as-fabricated 18Ni300

Element, wt.%	Ni	Mo	Co	Ti	Cr	C	Si	Mn
Powder	17.8	4.5	8.6	1	0.11	<0.01	<0.032	0.002

Table 2. Formation process parameters of the 18Ni300 powder

Laser power (W)	Scanning speed (mm/s)	Path spacing (mm)	Layer thickness (μm)
270	1,000	0.11	50
300	1,000	0.11	50
330	1,000	0.11	50
360	1,000	0.11	50

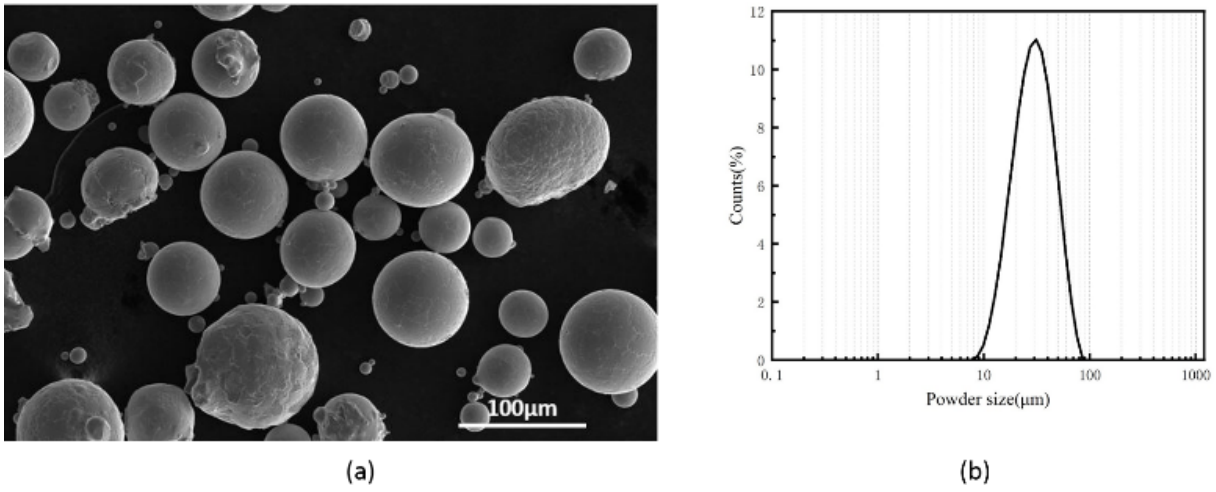


Fig. 1. SEM (A) and particle size distribution (B) of 18Ni300 powder

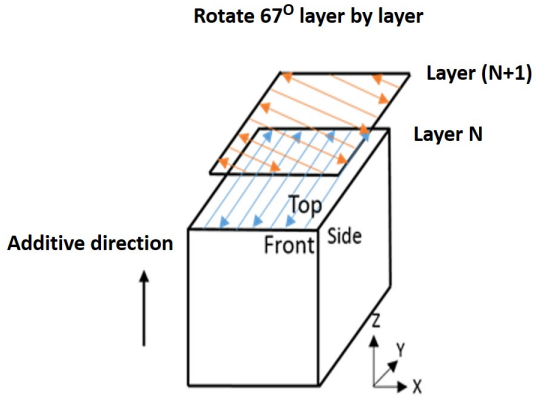


Fig. 2. Illustration of the laser scanning strategy

refined after heat treatment, forming dense acicular martensite, fuzzy and irregular grain boundary, and a large number of fine point austenite [18].

Martensitic steels contain more alloying elements. The solid solution treatment is usually carried out at about 810°C to obtain γ-austenite and to get ready for the microstructure of the age precipitated strengthening phase [19]. Solid solution treatment, aging treatment (480–500°C), and isothermal treatment (3–6 h) are carried out immediately to promote the preprecipitation of abundant fine dispersed intermetallic compounds (e.g., Ni3Mo, Ni3Ti, and Fe2Mo) on the martensitic matrix and can improve the material strength by 1,000–2,000 MPa [20, 21]. SLM can reduce the segregation caused by short-time high-speed local heat input and inhibit the development of the non-equilibrium phase. Therefore, M300 steel directly formed by SLM can maximize the strengthening effect of alloying elements [22, 23].

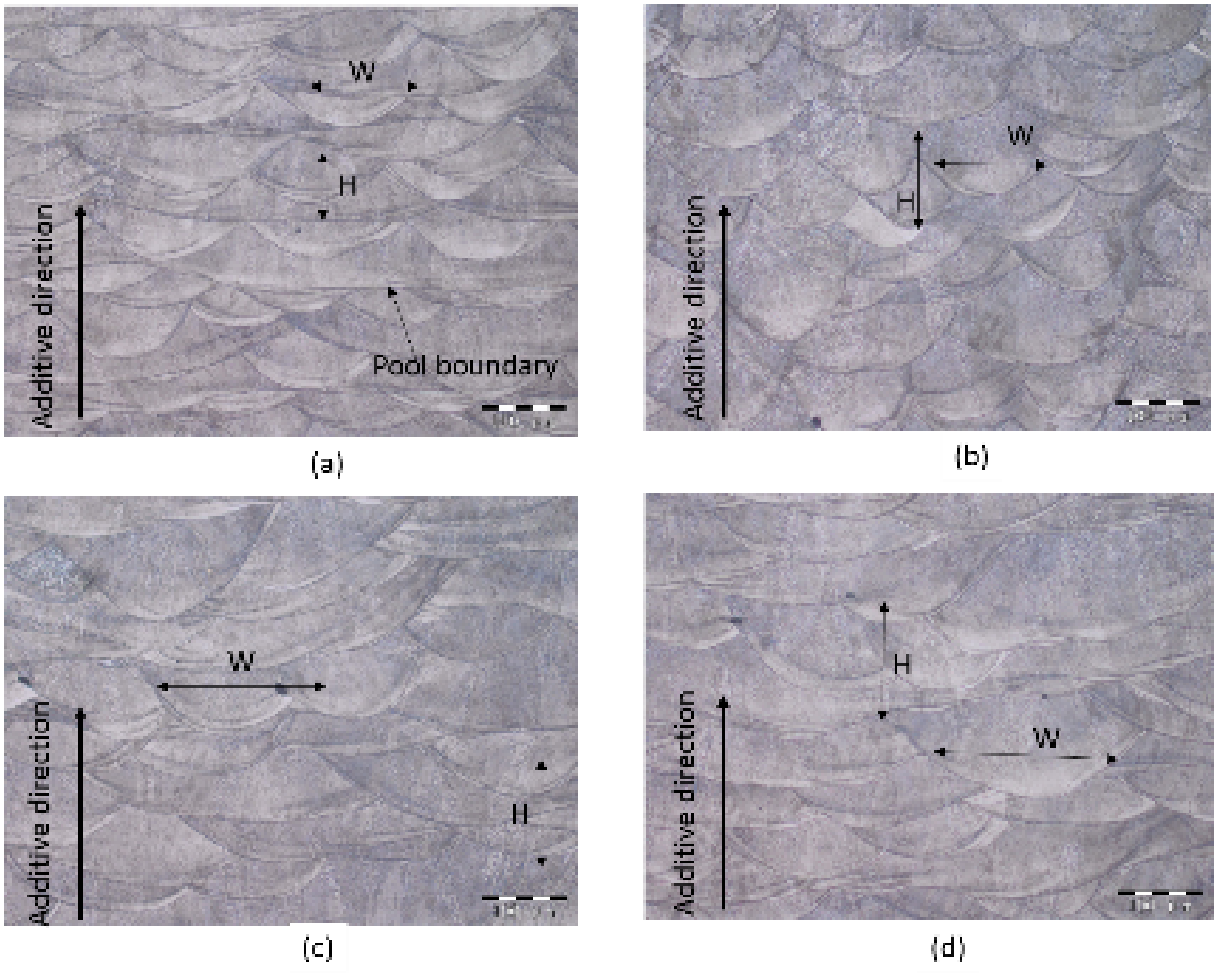


Fig. 3. Microstructure of the longitudinal section under different laser powers: (A): 270 W, (B) 300 W, (C) 320 W, and (D) 360 W

In the process of SLM, the process parameters critically influence the properties of the specimen. In this study, 18Ni300 martensitic steel was prepared using SLM, and the effects of laser power on the microstructure and mechanical properties of the specimens were investigated.

2. Materials and methods

Relevant experiments were carried out using an SLM-100 equipment, which had the maximum size of 100 mm $\times$ 100 mm $\times$ 100 mm. The maximum laser power is 500 W. During the formation process, high-purity argon $\geq$ 99.99% is used as the shielding gas, and the volume fraction of oxygen in the formation chamber is maintained $<$0.08%. Preparation: 10 mm $\times$ 10 mm $\times$ 10 mm of the sample was observed for microscopic morphology, and the relative density of the sample was measured using the drainage method. The GP-TS2000M electronic universal material testing machine was used. The tensile curves of maraging steel samples under different conditions were tested according to GB/T228.1-2010. An HV-1000 microhardness tester was used to measure the hardness of square samples under different process parameters at a loading load of 0.5 kg. Five points were randomly selected, and the average value was taken after the extreme value was removed from the test results. The tensile properties of specimens at

different laser powers were tested at room temperature using a tensile rate of 0.02 mm/s and a gauge length of 25 mm extensometer.

The 18Ni300 maraging alloy (1.2709) gas-atomized powder provided by Sandvik Osprey Co., Ltd. (Neath, UK) was used. Its chemical composition is shown in Table 1. The powder morphology and particle size distribution are shown in Figure 1. The D10, D50, and D90 of 18Ni300 powder are 19.0 μm, 38.1 μm, and 68.9 μm, respectively. The scanning strategy used in the experiment is shown in Figure 2. Four groups of 3D printing samples with different laser powers were prepared, and the optimal formation process parameters were selected, as shown in Table 2.

3. Results and discussion

3.1. Research and analysis of formation technology

Figure 3 shows the optical microstructure of the longitudinal section of the formed part at different laser powers. The laser beam scanned the metal powder at an angle of 90° to form molten pools, and the interaction between the molten pools formed a fish scale interface. When it was cooled to the martensite transformation temperature, part of austenite rapidly transformed into martensite. However, in the solidification process, solute elements easily microsegregated at the grain boundary, which hindered the martensitic transformation and caused residual austenite at the grain boundary. With the increase in laser power, the laser energy absorbed by the powder increased in short time, so the actual overlap ratio of adjacent welds increased. Also, the weld bead depth h and the width W increased.

A hardness changing curve 4 were obtained. The law of the side surface hardness was the same as that of the upper surface hardness (Figure 4). Under the same laser power, the side hardness of the specimen was higher than that of the upper surface hardness. This was because in the layer-by-

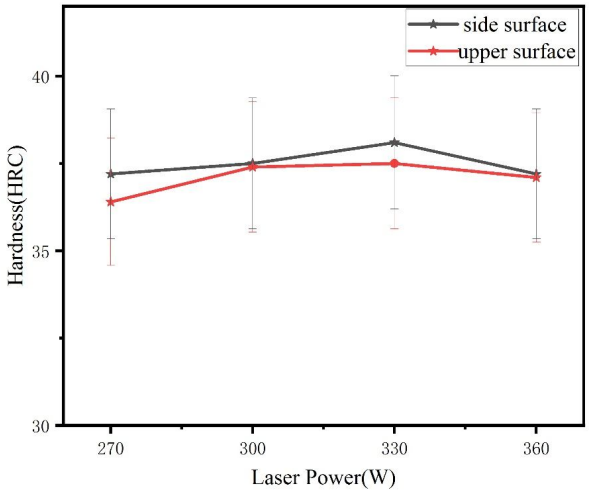


Fig. 4. Effect of laser power on surface hardness

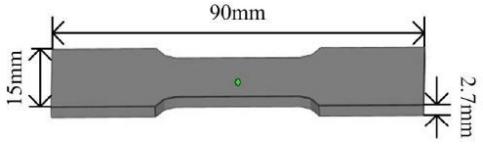


Fig. 5. Standard stretch piece

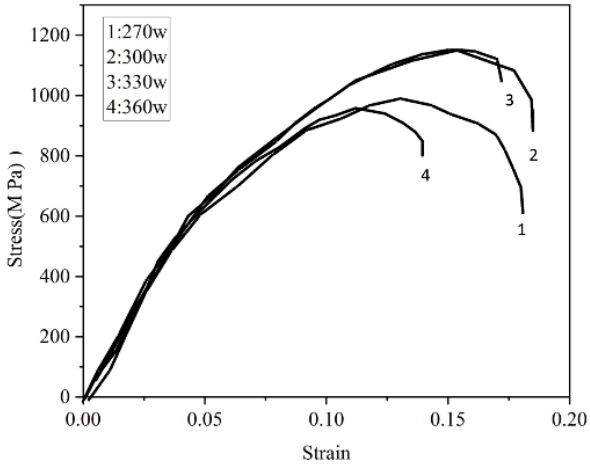


Fig. 6. Stress–strain curves under different laser powers

Table 3. Performance comparison under different laser powers

Laser power (W)	Rm (MPa)	Rp0.2 (MPa)	εPa 2
270	1,104	1,158	15.1
300	1,106	1,060	17.6
330	990	883	16.2
360	959	866	14.7

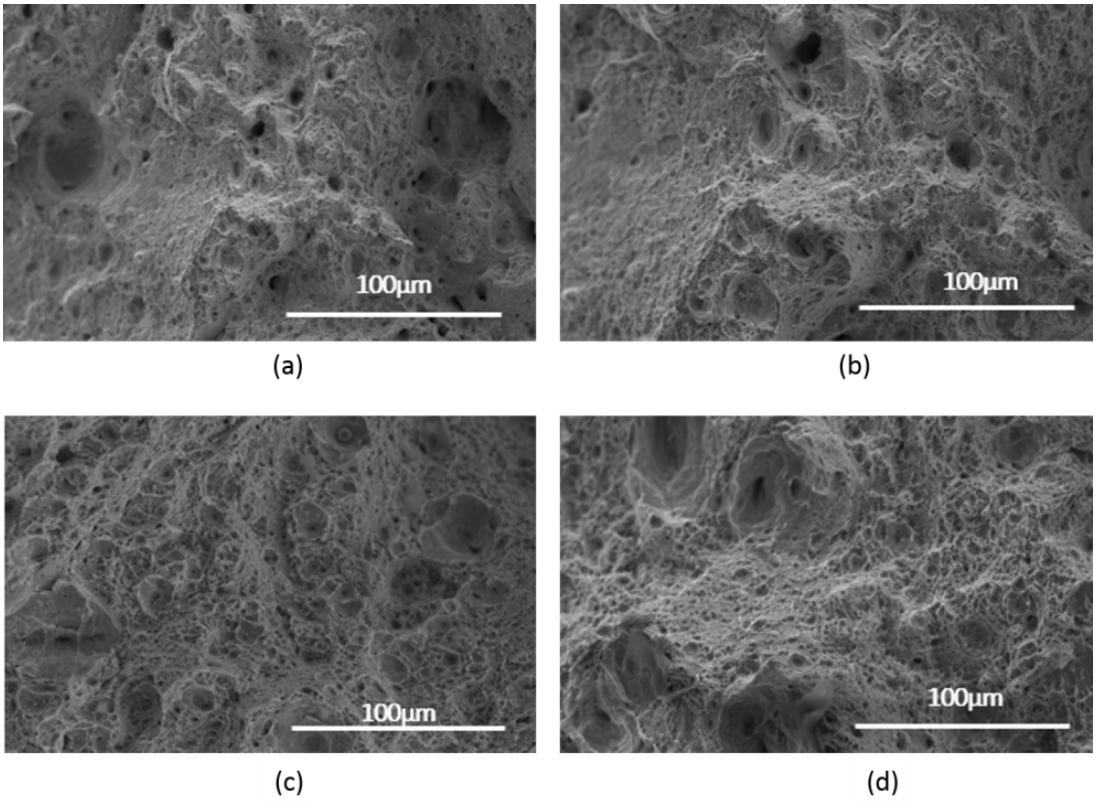


Fig. 7. Tensile fracture morphology of printed samples under different laser powers: (A) 270 W, (B) 300 W, (C) 320 W, and (D) 360 W

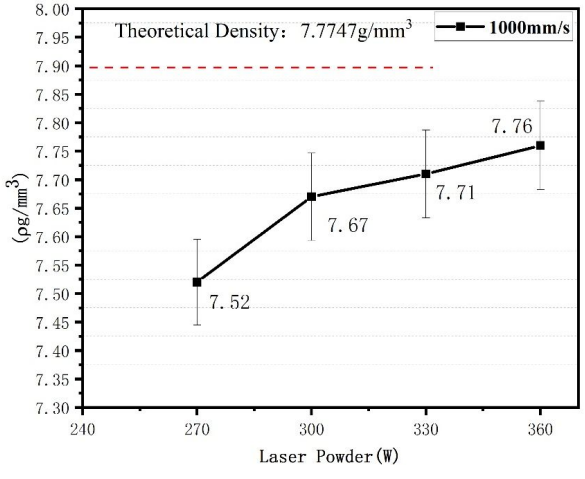


Fig. 8. Density variation under different laser powers

layer stacking, the formed martensite structure extended to the epitaxial boundary of the weld channel along the formation direction.

3.2. Research on molding process

The tensile parts were prepared according to GB/T 228.1-2010 (Figure 5). The engineering stress–strain curves of materials in different states are shown in Figure 6. From the curves, it can be seen that the slope of the elastic deformation stage of specimens under different laser powers is very small but with similar Young's modulus values. The tensile properties of 3D-printed pieces prepared with different laser powers are shown in Table 3. The tensile strength of 330 W and 300 W samples is the highest, but 300 W samples have higher elongation after fracture, showing good plasticity as well as micromorphology. Hence, the comprehensive mechanical properties of the samples are the best when the laser power is 300 W.

The fractures of tensile specimens were observed using SEM to further study the mechanism of tensile fractures. The fractured surface of the tensile specimens is composed of dimples in dif-

ferent sizes (Figure 7) due to the influence of energy density. When the laser power is 270 W, although the internal grain size is gradually refined and the grain boundary is increased, the crack propagation is hindered to some extent. However, due to the low power density, many defects appear in the formation process. In addition to deep holes in the tensile fractures, large particle inclusions appear in the holes. When the laser power is 300 W, a large number of equiaxed crystals are distributed on the fracture surface (Figure 7A). These depressions are evenly distributed and deep, showing high plasticity (Figure 7B). Therefore, the tensile strength and elongation of the samples are the highest. When the laser power is 330 W, the dimple size and depth of the fracture surface increase gradually. The fracture surface also has obvious tear marks, which reduce the tensile property (Figure 7C). When the laser power is increased to 360 W (Figure 7D), the surface dimples increase, and granular inclusions appear on the fracture surface, so the fracture mode changes to a plastic fracture.

3.3. Characterization of microstructure under optimized process parameters

Density is an important influence factor on the mechanical properties of samples formed using SLM. The optimization of laser process parameters during SLM is also the first step in the research of SLM additive manufacturing. Figure 8 shows the density curve of the formed samples with laser power when the laser scanning speed is constant. The curves show that the density is significantly positively correlated with the laser power, meaning the energy density increases with the increasing density of samples.

Based on the relative density measurements of the formed samples in the process optimization experiment, the optimized process of SLM and additive to martensitic stainless steel was determined. The laser power of 300 W was selected as the optimal process parameter. The surface of the sample was observed by SEM. Obvious grain boundaries appeared in the molten pool, and the microstructure of the central area was mainly cellular crystal (Figure 9). The formation of such crystals is mainly related to the cooling rate. A faster cooling rate can more promote the transformation of the initially generated planar crystal to the cell crystal. During SLM, the powder is heated and melted into molten metal. When the metal melt is continuously deposited to the crystal core, grains continue to grow, so the molten metal is solidified [21]. According to the hall patch relationship, the grain size is inversely proportional to the material strength. The fine grain structure of martensitic stainless steel indicates that the material has high strength, which is consistent with the previous tensile property results.

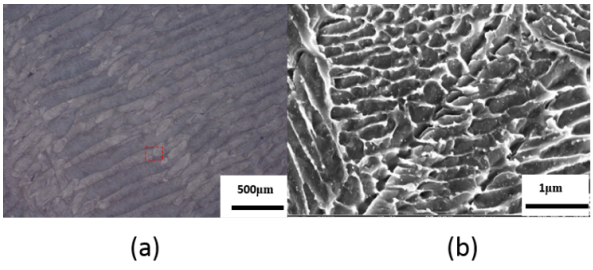


Fig. 9. SEM image (A) and local magnification (B) of the upper surface of the sample

Figure 10 shows a microstructure diagram of EBSD on the upper surface of a sample with a laser power of 300 W and 360 W. The upper surface EBSD inverse pole diagram (IPF) of 300 W (Figure 10A) shows that the columnar crystal grains exhibit weak texture due to the high thermal gradient. The formation of columnar crystals is caused by the high temperature gradient along the growth direction during SLM formation [22]. Moreover, the upper surface EBSD grain boundary diagram of 300 W (Figure 10A1) shows many small-angle grain boundaries in the upper surface, reflecting the thermal stress caused by rapid heating and cooling, and the formed sample has a high dislocation density [23]. The grain size of the sample is <10 μm (Figures 10A and 10A1), which imply that the sample of 300 W has better tensile properties than the sample of 360 W (Figures 10B and 10B1).

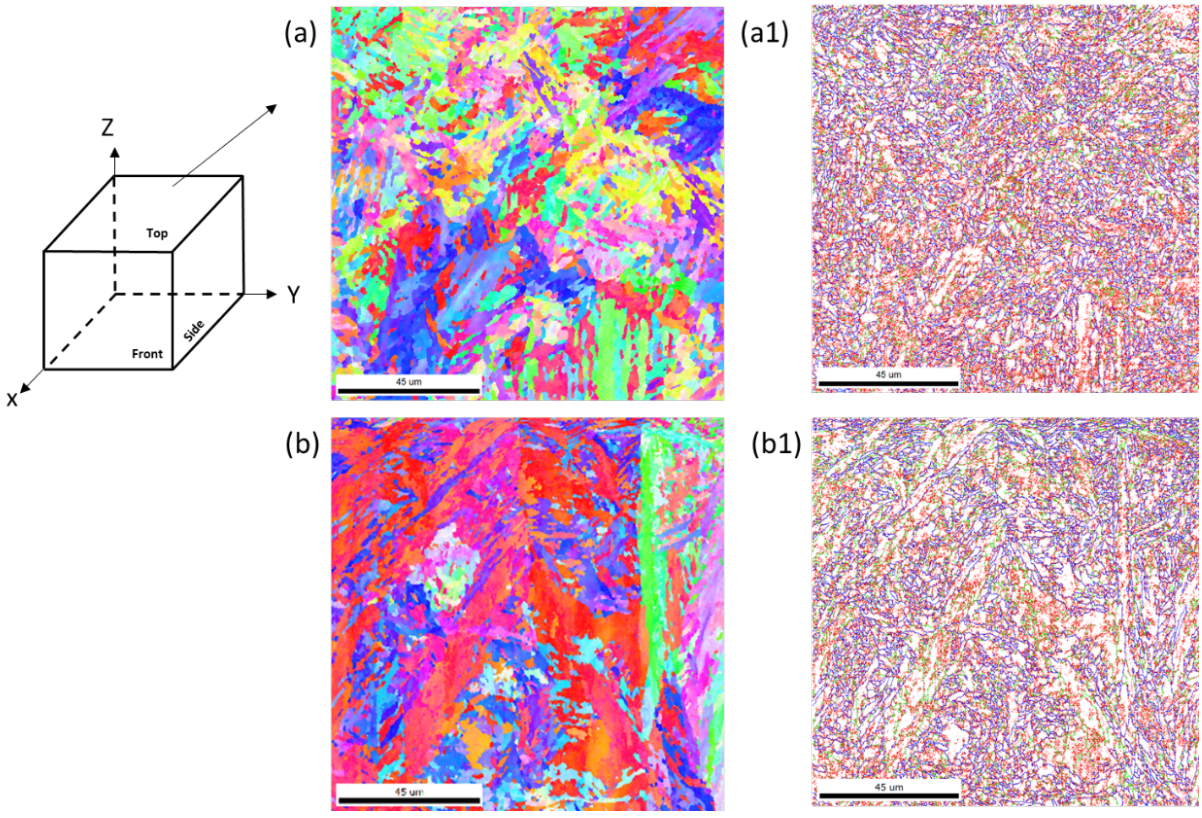


Fig. 10. Microstructure analysis of EBSD on the upper surface of the sample: (A) IPF maps of 300 W, (A1) GB maps of 300 W; and (B) IPF maps of 360 W, (B1) GB maps of 360 W. IPF, inverse pole diagram

4. Conclusions

The basic process of SLM-formed martensitic stainless steel was studied, and the influence of laser power on the microstructure, relative density, and mechanical properties was analyzed. The optimal laser process parameters were determined to be a laser power of 330 W and a scanning speed of 1,000 mm/s.

1. The microstructure under different laser powers shows that with the increase in laser power, the grain size of the cladding layer becomes smaller and fine equiaxed crystal, and the structure is more compact.
2. The variation law of side hardness under different laser powers is the same as that of the upper surface hardness. The side hardness of the printed sample under the same laser power is higher than that of the upper surface hardness. The tensile strength curve shows a "low–high–low" distribution trend. When the laser power is 300 W, the comprehensive mechanical properties of the sample are the best as the tensile strength, microhardness, elongation at break, and elongation after the fracture are 1,217 MPa, 37.5%, 37.6%, and 8.93%, respectively.
3. When the laser power is 300 W and the scanning speed is 1,000 mm/s, the EBSD on the upper surface shows that the columnar crystal grains have weak texture with many small-angle grain boundaries, and the grain size is <10 μm. These results reflect the excellent mechanical properties of martensitic stainless steel to some extent.

Acknowledgements

We thank the timely help given by the Shanghai Jiao Tong University School of Medicine (Jyh1820).

References

[1] Tan C, Zhou K, Ma W, Zhang P, Liu M, Kuang T. Microstructural evolution, nanoprecipitation behavior and mechanical properties of selective laser melted high-performance grade 300 maraging steel. Mater Des. 2017;134:23–34.

[2] Bhardwaj T, Shukla M. Effect of laser scanning strategies on texture, physical and mechanical properties of laser sintered maraging steel. Mater Sci Eng. 2018;734:102–9.

[3] Debroy T, Wei HL, Zuback JS, Mukherjee T, Elmer JW, Milewski JO, et al. Additive manufacturing of metallic components – Process, structure and properties. Prog Mater Sci. 2018;92:112–224.

[4] Wang Z, Beese AM. Stress state-dependent mechanics of additively manufactured 304L stainless steel: part 1-characterization and modeling of the effect of stress state and texture on microstructural evolution. Mater Sci Eng A. 2019;743:811–23.

[5] Choo H, Sham KL, Bohling J, Ngo A, Xiao X, Ren Y, et al. Effect of laser power on defect, texture, and microstructure of a laser powder bed fusion processed 316L stainless steel. Mater Des. 2018;164:107534.

[6] Takajo S, Brown DW, Clausen B, Gray III GT, Knapp CM, Martinez DT, et al. Spatially resolved texture and microstructure evolution of additively manufactured and gas gun deformed 304L stainless steel investigated by neutron diffraction and electron backscatter diffraction. Powder Diff. 2018;33(2):141–6.

[7] Gribbin S, Ghorbanpour S, Ferreri NC, Bicknell J, Tsukrov I, Knezevic M. Role of grain structure, grain boundaries, crystallographic texture, precipitates, and porosity on fatigue behavior of Inconel 718 at room and elevated temperatures. Mater Charact. 2019;149:184–97.

[8] Popovich VA, Borisov EV, Popovich AA, Sufiiarov V.sh, Masaylo DV, Alzina L. Functionally graded Inconel 718 processed by additive manufacturing: crystallographic texture, anisotropy of microstructure and mechanical properties. Mater Des. 2017;114:441–9.

[9] Geiger F, Kunze K, Etter T. Tailoring the texture of IN738LC processed by selective laser melting (SLM) by specific scanning strategies. Mater Sci Eng A Struct Mater Prop Misrostruc Process. 2016;661:240–6.

[10] Honnige JR, Colegrove PA, Ahmad B, Fitzpatrick ME, Ganguly S, Lee TL, et al. Residual stress and texture control in Ti-6Al-4V wire + arc additively manufactured intersections by stress relief and rolling. Mater Des. 2018;150:193–205.

[11] Sridharan N, Chaudhary A, Nandwana P, Babu SS. Texture evolution during laser direct metal deposition of Ti-6Al-4V. J Miner Met Mater Soc. 2016;68(3):1–6.

[12] Hrabe N, White R, Lucon E. Effects of internal porosity and crystallographic texture on Charpy absorbed energy of electron beam melting titanium alloy (Ti-6Al-4V). Mater Sci Eng A. 2018;742:269–77.

[13] Kučerová L, Zetková I, Jandová A, Bystrianský M. Microstructural characterisation and in-situ straining of additive-manufactured X3NiCoMoTi 18-9-5 maraging steel. Mater Sci Eng A. 2019;750:70–80.

[14] Bai Y, Zhao C, Wang D, Wang H. Evolution mechanism of surface morphology and internal hole defect of 18Ni300 maraging steel fabricated by selective laser melting. J Mater Process Technol. 2022;299:117328.

[15] Riccardo C, Jannis NL, Ausonio T, Maurizio V. Aging behaviour and mechanical performance of 18-Ni 300 steel processed by selective laser melting. Met Open Access Metall J. 2016;6(9):218.

[16] Y Kawabe, K Nakazawa, M Kanao, S Muneki. Delayed failure crack and fracture toughness of 18 Ni maraging steel with aging structure at low temperature. Tetsu-to-Hagane. 2010;60(12):1613–23.

[17] Yang K, Qu WS, Kong FY, Su GY. Effects of solution treatment temperature on grain growth and mechanical properties of high strength 18%Ni cobalt free maraging steel. Mater Sci Technol. 2003;19(1):117–24.

[18] Z Jie, L Shuai Q Wei, Y Shi, L Wang, L Guo. Cracking behavior and inhibiting process of inconel 625 alloy formed by selective laser melting. Rare Met. 2015:39(011):961-966.

[19] Kempen K, Yasa E, Thijs L, Kruth JP, Van Humbeeck J. Microstructure and mechanical properties of selective laser melted 18Ni-300 steel. Phys Procedia. 2011;12:255–63.

[20] Sohail M, Han SW, Na SJ, Gumenyuk A, Rethmeier M. Characteristics of weld pool behavior in laser welding with various power inputs. Weld World. 2014;58(3):269–77.

[21] Loulou T, Artyukhin EA, Bardon JP. Estimation of thermal contract resistance during the first stages of metal solidification process: II—experimental setup and results. Int J Heat Mass Transfer. 1999;42(12):2129–42.

[22] Zhou X, Li K, Zhang D, Liu X, Ma J, Liu W, et al. Textures formed in a CoCrMo alloy by selective laser melting. J Alloys Compd. 2015;631:153–64.

[23] Kajima Y, Takaichi A, Kittikundecha N, Nakamoto T, Kimura T, Nomura N, et al. Effect of heat-treatment temperature on microstructures and mechanical properties of Co–Cr–Mo alloys fabricated by selective laser melting. Mater Sci Eng A. 2018;726:21–31.

Received 2022-09-20
Accepted 2022-11-25